

Flow-induced vibrations of three circular cylinders in an equilateral triangular arrangement subjected to cross-flow

Weilin Chen¹, Chunling Ji^{*1,2}, Md. Mahbub Alam³ and Dong Xu¹

¹State Key Laboratory of Hydraulic Engineering Simulation & Safety, Tianjin University, Tianjin, 300072, China

²Collaborative Innovation Centre for Advanced Ship and Deep-Sea Exploration, Shanghai 200240, China

³Institute for Turbulence-Noise-Vibration Interaction and Control, Harbin Institute of Technology (Shenzhen), Shenzhen 518055, China

(Received September 7, 2018, Revised February 26, 2019, Accepted February 28, 2019)

Abstract. Vortex-induced vibration of three circular cylinders (each of diameter D) in an equilateral triangular arrangement is investigated using the immersed boundary method. The cylinders, with one placed upstream and the other two side-by-side downstream, are free to vibrate in the cross-flow direction. The cylinder center-to-center spacing L is adopted as $L/D = 2.0$. Other parameters include the Reynolds number $Re = 100$, mass ratio $m^* = 2.0$, reduced velocity $U_r = 2 \sim 15$ and damping ratio $\zeta = 0$. Cylinder vibration responses are dependent on U_r and classified into five regimes, i.e. Regime I ($U_r \leq 3.2$), Regime II ($3.2 < U_r \leq 5.0$), Regime III ($5.0 < U_r \leq 6.4$), Regime IV ($6.4 < U_r \leq 9.2$) and Regime V ($U_r > 9.2$). Different facets of vibration amplitude, hydrodynamic forces, wake patterns and displacement spectra are extracted and presented in detail for each regime.

Keywords: vortex-induced vibration; circular cylinder; triangular arrangement; immersed boundary method

1. Introduction

Vortex-induced vibration (VIV) of cylindrical structures, as a canonical fluid-structure interaction (FSI) problem, has been extensively investigated in the past several decades (Ji *et al.* 2011, 2018a, Qin *et al.* 2017, 2018, Bhat and Alam 2018). Notably, the VIV of an isolated circular cylinder in cross-flow has received much attention (Williamson and Govardhan 2004, Sarpkaya 2004, Blevins 1990, Kim *et al.* 2018). However, many engineering applications, such as bundles of heat exchangers, marine risers, transmission lines, undersea pipelines, involve multiple cylinders, and the interactions existing between the structures are complicated (Alam *et al.* 2014, Chen *et al.* 2015a, 2015b, 2018, Kim *et al.* 2016, Alam 2016, Ji *et al.* 2018b). In the present paper, we investigate the VIV of three equilateral-triangular-arranged circular cylinders subjected to a laminar cross-flow, and explore the characteristics of vibration responses, wakes, and hydrodynamic forces.

Considering the applications of multiple cylinders, the flow around two fixed rigid cylinders has been extensively investigated. Zdravkovich (1977) classified the two-cylinder flow interference into proximity interference, wake interference, and combined interference. The proximity interference occurs when two staggered (or side-by-side) cylinders are close enough to interact with each other or when the downstream cylinder is entirely embraced by the shear layers separated from the upstream cylinder. The wake interference occurs when two cylinders are tandem or nearly tandem and relatively far from each other, such that

fully developed vortices from the upstream cylinder come into being in the gap between the two cylinders. The combined interference can be found in an overlapped region between proximity and wake interferences.

King and Johns (1976) investigated the interference between two elastically-supported circular cylinders in tandem for $1 \times 10^3 < Re < 2 \times 10^4$, where Re is the Reynolds number based on freestream velocity U_∞ and cylinder diameter D . The upstream cylinder showed typical VIV characteristics while the downstream cylinder's vibration response was more complicated. Wake galloping vibration of the downstream cylinder occurred at a small streamwise spacing ratio $L/D = 2.5$ (L is the cylinder center-to-center spacing) and large reduced velocity U_r (> 11) while the upstream cylinder vibration was negligible. The wake galloping was absent at a larger $L/D = 5.5$. Hover and Triantafyllou (2001) at $Re = 3 \times 10^4$ studied the vibration and force responses of a two-dimensional cylinder behind a stationary upstream cylinder with $L/D = 4.75$ in a towing tank. Large-amplitude wake galloping response sustained $U_r > 17$. When the stagger angle α was increased from 0° (tandem) to 12° , the normalized transverse vibration amplitude Y/D reduced from 1.9 to 1.4, still showing a divergent trend. Assi *et al.* (2006) at $3 \times 10^3 < Re < 1.3 \times 10^4$ carried out flume experiments on the wake-induced vibration (WIV) of an elastically mounted rigid cylinder in the near-wake of an upstream stationary cylinder. Wake galloping was observed in the range of $2 < L/D < 5.6$. Assi *et al.* (2010, 2013) at $2 \times 10^3 < Re < 3 \times 10^4$ reported a combined vortex resonance and wake galloping response of the downstream cylinder when L/D was small. A typical vortex resonance response was detected when the spacing ratio was as large as $L/D = 20$.

Kim *et al.* (2009) examined the interference between two elastically mounted tandem cylinders for $Re = 4.3 \times 10^3$

*Corresponding author, Professor
E-mail: cnji@tju.edu.cn

$\sim 7.4 \times 10^4$, $L/D = 1.1 \sim 4.2$ with a small increment of $\Delta L/D = 0.1$. Five vibration regimes were identified. The downstream cylinder showed VIV-like response, while the upstream cylinder underwent VIV and galloping at different L/D . Alam and Kim (2009) for the same Re range systematically investigated flow-induced vibrations of two elastically mounted staggered cylinders. Seven vibration patterns were observed depending on L/D and α . Alam and Meyer (2013) presented a useful map of cylinder responses in the parametric range of $L/D = 1.1 \sim 6.0$ and $\alpha = 0^\circ \sim 180^\circ$ by compiling the vibration response data of two elastically mounted cylinders in cross-flow from the experimental studies of Bokaian and Geoola (1984a, 1984b), Kim et al. (2009), Alam and Kim (2009). It was found that galloping (upstream cylinder) and/or wake galloping (downstream cylinder) vibrations existed only in a small 'mushroom-like' region $L/D = 1.23 \sim 3.5$ and $\alpha = 0^\circ \sim 20^\circ$. Qin *et al.* (2018) examined vibration responses of two freely vibrating tandem cylinders of different natural frequencies for $L/D = 1.5$ and 2.0 . A critical U_r in the galloping vibration regime was identified where the vibration amplitude of the downstream cylinder drastically jumps and that of the upstream cylinder drops. The jump/drop was linked to a lock-in of the vortex shedding with the fifth harmonics of the downstream cylinder natural frequency. Kim and Alam (2015) examined the flow-induced vibrations of two side-by-side cylinders and identified four vibration patterns depending on L/D .

As to three cylinders, Yu *et al.* (2016) at $Re = 100$ and 150 numerically investigated the VIV of three tandem cylinders with a cylinder mass ratio $m^* = 1.27$, $L/D = 4.0$ and $U_r = 2 \sim 13$. Compared to that of two tandem cylinders, the maximum transverse amplitude was increased by about 25% with the maximum streamwise amplitude reaching $1.3D$. The displacement trajectories of three cylinders showed "bounded random movements" even in two-dimensional flows. Chen *et al.* (2018) numerically studied the VIV of three tandem cylinders for a wide parametric space of $L/D = 1.2 \sim 5.0$ and $U_r = 3 \sim 80$. All three cylinders were constrained to vibrate in the transverse direction. Galloping-like vibration existed for a small $L/D (= 1.2)$ and VIV-like response occurred in moderate and large $L/D (= 1.5 \sim 5.0)$. Behara *et al.* (2017) numerically investigated the VIV of three cylinders in a triangular arrangement at $Re = 60 \sim 160$, with one cylinder upstream and the other two downstream cylinders side-by-side. The transverse center-to-center distance of two downstream cylinders was $3.0D$ and the streamwise distance between the centers of the upstream and downstream cylinders was $5.0D$. Three cylinders were free to vibrate in both streamwise and transverse directions. Due to the large L/D , the response of the upstream cylinder was similar to that of an isolated cylinder, showing initial and lower branches. However, three branches, i.e., initial, upper and lower, were observed on the downstream cylinders.

Based on the above review, it can be seen that the VIV of three cylinders in the equilateral triangular arrangement involves complex flow dynamics but has been scarcely investigated. In this paper, we focus on the VIV of three equally-spaced cylinders at a small spacing ratio $L/D = 2.0$,

where the interaction between the cylinders is fierce. The rest of this paper is organized as follows. In Section 2, the adopted numerical method and its validation are given. In Section 3, vibration amplitude and frequency, hydrodynamic forces and equilibrium position of three equilateral-triangular-arranged circular cylinders undergoing VIV are presented, together with the near-wake patterns. In Section 4, the main conclusions are provided.

2. Numerical methodology and validation case

The numerical simulations are carried out by using an in-house CFD code – CgLES_IBM. The governing equations for the fluid flow are the incompressible Navier–Stokes equations. The two-step predictor-corrector procedure is adopted for the decoupling of the flow governing equations. The resultant pressure Poisson equation is solved by using the BiCGSTAB scheme, together with the geometric multi-grid preconditioner. The second-order Adams-Bashforth time marching scheme is employed to calculate a new velocity field.

The dynamics of the elastically supported circular cylinders is simplified as a mass-damper-spring system. The governing equations for cylinder motion are based on Newton's Second Law and are simply solved by using the standard Newmark- β method with the second-order temporal accuracy. In this study, the cylinders are free to oscillate in the cross-flow direction.

The fluid-structure interaction is simulated by using the immersed boundary (IB) method which was first introduced by Peskin (1972) in the simulation of blood flow around the flexible leaflet of a human heart. In the framework of the IB method, the flow governing equations are discretized on a fixed Cartesian mesh, which generally does not conform to the geometry of moving solids. As a result, the boundary conditions at the fluid-cylinder interface cannot be imposed directly. Instead, an extra body force is added into the momentum equation by using interpolation and distribution functions to take such interaction into account. For the sake of conciseness, details of the methodology are not presented, and readers are referred to our previous work (Ji *et al.* 2012, Chen *et al.* 2015a) for details.

In the simulations of VIV of three equilateral-triangular-arranged circular cylinders, the streamwise and transverse lengths of the computational domain are both $200D$, as shown in Fig. 1. The three cylinders are indexed as 1, 2 and 3, respectively. To improve the accuracy of the numerical results, the cylinders are covered by a rectangle region $8D \times 8D$ discretized by a uniform mesh with a grid spacing of $D/64$ in the streamwise and transverse directions. Beyond the region, a stretched mesh is adopted to keep the total grid number within an affordable range. A similar configuration was applied in our previous simulations (Chen *et al.* 2015b, 2018). The boundary conditions are set as follows. A Dirichlet-type boundary condition is adopted at the inflow and a Neumann-type boundary condition is employed at the outflow. The top and bottom walls are set as free-slip boundaries. The non-dimensional time step $\Delta t U_\infty / D$ is 0.004. In the simulations, the cylinders start to vibration

Table 1 Comparison of the VIV of three circular cylinders with $\Delta t U_\infty / D = 0.004$ and different grid spacings. \bar{C}_d is the time-averaged drag coefficient. C'_d and C'_l are the r.m.s. of drag and lift coefficients, respectively. A_y/D is the normalized vibration amplitude in the transverse direction. St is the Strouhal number. The values in parentheses indicate the differences in percentage. The results of Cylinder 3 are not listed as identical to those of Cylinder 2

	$\Delta x/D (= \Delta y/D)$	\bar{C}_d	C'_d	C'_l	A_y/D	St
Cylinder 1	1/32	1.136(2.2)	0.252(0)	0.748(7.6)	0.648(0.2)	0.122(1.6)
	1/64	1.156(0.4)	0.247(0.8)	0.702(1.0)	0.641(1.2)	0.124(0)
	1/128	1.161	0.252	0.695	0.649	0.124
Cylinder 2	1/32	1.432(3.2)	0.555(5.9)	0.718(9.3)	0.688(2.1)	0.122(1.6)
	1/64	1.405(1.3)	0.530(1.1)	0.662(0.8)	0.672(0.3)	0.124(0)
	1/128	1.387	0.524	0.657	0.674	0.124

Table 2 Comparison of the VIV of three circular cylinders with $\Delta x/D (= \Delta y/D) = 1/64$ and different time steps.

	$\Delta t U_\infty / D$	\bar{C}_d	C'_d	C'_l	A_y/D	St
Cylinder 1	0.006	0.155(0.5)	0.242(2.9)	0.689(2.3)	0.633(2.0)	0.124(1.6)
	0.004	1.156(0.4)	0.247(0.8)	0.702(0.4)	0.641(0.8)	0.124(1.6)
	0.002	1.161	0.249	0.705	0.646	0.126
Cylinder 2	0.006	1.399(0.5)	0.526(1.3)	0.650(0.5)	0.662(1.2)	0.124(1.6)
	0.004	1.405(0.1)	0.530(0.6)	0.662(2.3)	0.672(0.3)	0.124(1.6)
	0.002	1.406	0.533	0.647	0.670	0.126

Table 3 Comparison of the VIV of three circular cylinders in an isosceles triangle arrangement. A_x/D is the normalized vibration amplitude in the streamwise direction

		C'_d	C'_l	A_x/D	A_y/D	St
Cylinder 1	B17	0.256	0.175	0.031	0.571	0.154
	Present	0.260(1.6)	0.173(1.1)	0.030(3.2)	0.572(0.2)	0.154(0)
Cylinder 2	B17	0.506	0.729	0.458	0.922	0.146
	Present	0.500(1.2)	0.740(1.5)	0.450(1.7)	0.913(1.0)	0.146(0)
Cylinder 3	B17	0.510	0.723	0.455	0.928	0.145
	Present	0.509(0.2)	0.753(4.1)	0.446(2.0)	0.913(1.6)	0.146(0.7)

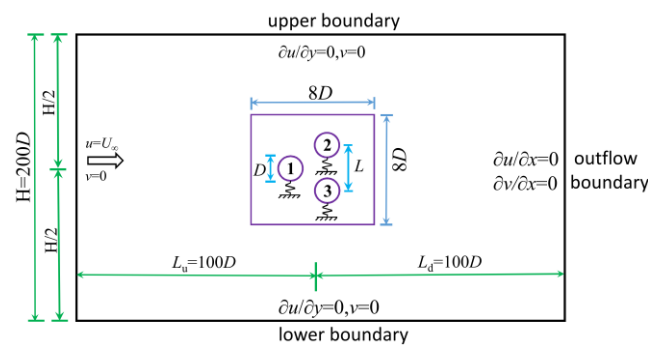


Fig. 1 The computational domain and boundary conditions

from the rest. Each simulation is carried out for more than 100 oscillation cycles after the vibrations are statistically stable. Other parameters are $m^* = 2.0$, $L/D = 2.0$, $Re = 100$ and the structural damping ratio $\zeta = 0$.

The adopted non-dimensional grid spacings ($\Delta x/D$, $\Delta y/D$) and time step ($\Delta t U_\infty / D$) are checked for VIV of three equally-spaced circular cylinders with $L/D = 2.0$, $U_r = 6.0$, $m^* = 2$ and $\zeta = 0$. Table 1 shows only marginal difference ($\leq 1.3\%$) between the results with $\Delta x/D (= \Delta y/D) = 1/64$ and

1/128, indicating the numerical results with $\Delta x/D (= \Delta y/D) = 1/64$ is grid-independent. Although the results with different $\Delta t U_\infty/D$ show no consistently convergent trend, the difference is sufficiently small ($< 2.3\%$) at $\Delta t U_\infty/D = 0.004$, as listed in Table 2. Based on the above, $\Delta x/D (= \Delta y/D) = 1/64$ and $\Delta t U_\infty/D = 0.004$ are adopted in the following study.

For validating the numerical methodology, the VIV of three circular cylinders in an isosceles triangle arrangement was simulated and the results were compared with those in Behara *et al.* (2017) (hereafter referred to as B17). The adopted parameters are same with those in B17. The center-to-center distance of the downstream cylinders is $3D$ while the streamwise spacing between the upstream cylinder and downstream cylinders is $5D$, with $Re = 100$, $U_r = 6.41$, $m^* = 10$ and $\zeta = 0$. The computational domain size is $L_u = 8D$, $L_d = 50D$ and $H = 25D$. It can be seen from Table 3 that the present results show excellent agreements with those in B17, with the maximum deviation being lower than 4.1% for C'_l .

3. Results and discussions

3.1 Regime partitions

The non-dimensional vibration amplitude A/D is defined as $A/D = \sqrt{2} y_{rms}/D$, where y_{rms} is the root-mean-square (r.m.s.) of transverse displacement. Figs. 2 and 3 show dependence on U_r of A/D , time-mean drag \bar{C}_d , fluctuating drag C'_d , time-mean lift \bar{C}_l , and fluctuating lift C'_l of the three cylinders. The magnitude of A/D , \bar{C}_d , C'_d , \bar{C}_l , and C'_l each is the same for the two downstream cylinders at different U_r , except for $U_r = 7.4 \sim 7.8$. The U_r -dependent response can be divided into five regimes, i.e. Regime I at $U_r \leq 3.2$, Regime II at $3.2 < U_r \leq 5.0$, Regime III at $5.0 < U_r \leq 6.4$, Regime IV at $6.4 < U_r \leq 9.2$ and Regime V at $U_r > 9.2$, which have distinct characteristics of A/D and hydrodynamic forces.

Regime I is featured by no-vibration of the three cylinders. The \bar{C}_d of the upstream cylinder is smaller than that of the downstream cylinders each. Small attractive \bar{C}_l exists, and C'_d and C'_l are very small.

In Regime II, the upstream cylinder keeps stationary while the downstream ones undergo a fast growth of A/D with increasing U_r . The \bar{C}_d decreases and increases for the upstream and downstream cylinders, respectively. Repulsive \bar{C}_l is examined on the downstream cylinders while the upstream cylinder $\bar{C}_l = 0$. The C'_d and C'_l of the upstream cylinder are invariant while those of the downstream cylinders behave differently, C'_d escalating and C'_l growing for $U_r = 3.2 \sim 4.0$ followed by a declination for $U_r = 4.0 \sim 5.0$. The \bar{C}_d , \bar{C}_l and C'_d each reaches its maximum at the border ($U_r = 5.0$) of this regime while the C'_l is maximum at $U_r = 4.0$.

With increasing U_r from Regime II to III, A/D of the upstream cylinder soars while A/D of the downstream cylinders shows a mild growing. Interestingly, the variations in A/D , \bar{C}_d , and C'_l of the upstream cylinder in

Regime III are quite similar to those of the downstream cylinder in Regime II. Repulsive \bar{C}_l persists for the downstream cylinders, decreasing with U_r , while $\bar{C}_l = 0$ for the upstream cylinder.

Fundamental changes are observed as U_r is increased from Regime III to IV, with A/D , \bar{C}_d , C'_d , \bar{C}_l , and C'_l all dipping for the three cylinders at $U_r = 6.6$. In Regime IV, the downstream cylinders' A/D keeps constant while the upstream cylinder's A/D augments linearly. The \bar{C}_d , C'_d , and C'_l level off for the upstream cylinder and decrease for the downstream cylinders. The \bar{C}_l , albeit small in magnitude, becomes attractive for the downstream cylinders. Note that at and around $U_r = 7.5$, the \bar{C}_l of either downstream cylinder is positive, indicating that the balanced positions of two downstream cylinders shift towards the same direction. As a result, the vibration amplitudes of two downstream cylinders are unequal. Asymmetric vibrations of two side-by-side cylinders were also found in Chen *et al.* (2015a, b).

Regime V, following Regime IV, is separated by drastic jumps in all parameters (A/D , \bar{C}_d , C'_d , \bar{C}_l , and C'_l) at the border. In Regime V, the upstream cylinder's A/D diminishes with increasing U_r while the downstream cylinders' A/D enlarges. This galloping-like vibration of the downstream cylinders, named as wake-induced galloping (WG), has been reported in the VIV of two tandem cylinders at high Reynolds numbers with low m^* (Assi *et al.* 2010) and high m^* (Alam and Meyer 2013). It was also found in the VIV of three tandem cylinders at low Reynolds numbers (Chen *et al.* 2018).

In general, it can be seen that the regimes have distinctive characteristics in both vibration amplitude and hydrodynamic forces, and the boundaries between two adjacent regions are well-defined.

Fig. 4 shows the normalized vibration frequencies f_y/f_n of three cylinders as a function of U_r , where f_y is the dominant frequency of the displacement, obtained from the fast Fourier transform of the cylinder displacements.

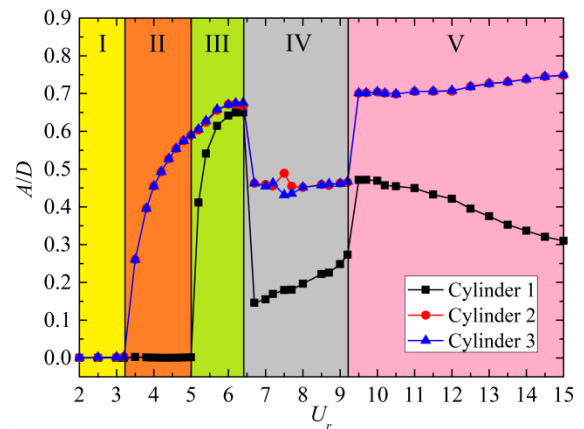


Fig. 2 Dependence on U_r of vibration responses of three cylinders

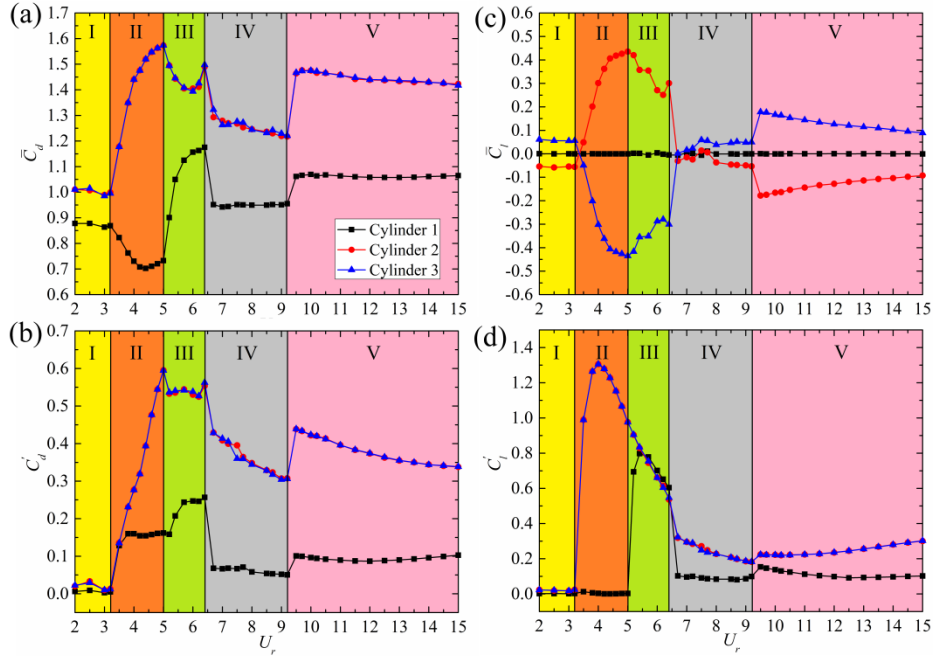


Fig. 3 Dependence on U_r of hydrodynamic forces on three cylinders

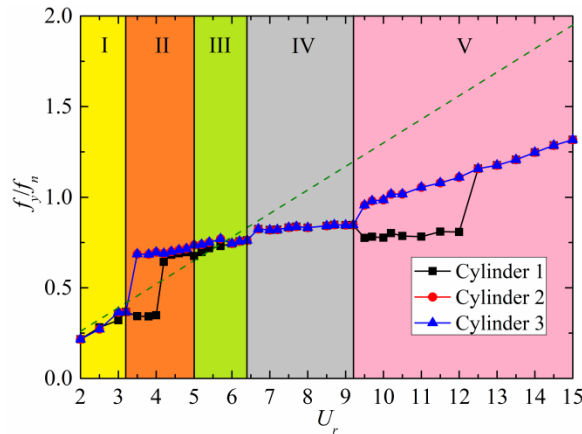


Fig. 4 The normalized vibration frequencies (f_y/f_n) of three cylinders. The dashed line denotes the normalized vortex-shedding frequency (f_v/f_n) of three stationary cylinders at $L/D = 2$

The variation of the normalized vortex-shedding frequency $f_v/f_n = StU_r$ is also superimposed for comparison, where f_v and St ($= 0.13$) are, respectively, the vortex-shedding frequency and Strouhal number of three stationary cylinders with $L/D = 2$ and $Re = 100$. In Regime I, f_y closely follows f_v , owing to no-vibration of the cylinders. The f_y/f_n of the downstream cylinders jumps at $U_r = 3.5$ and levels off approximately at $f_y/f_n = 0.75$ in Regimes II and III. However, the f_y/f_n of the upstream cylinder jumps at $U_r = 4.2$. In $U_r = 3.5 \sim 4.0$, the upstream cylinder's vibration frequency is half of the downstream ones. In Regime IV, three vibration frequencies are equivalent, keeping around $f_y/f_n = 0.8$. In the early part of Regime V ($U_r = 9.5 \sim 12.0$), the upstream cylinder vibrates at a lower frequency than the downstream cylinders. In the rest part ($U_r > 12.0$), the three cylinders again vibrate at the same frequency.

Fig. 5 presents the variations of the equilibrium positions \bar{y}/D of three cylinders versus U_r . The distance between the \bar{y}/D of two downstream cylinders increases in Regime II due to the repulsive \bar{C}_l , and keeps about $2.18D$ in Regime III. However, in Regime IV, the distance is slightly smaller than the initial spacing because of the small attractive \bar{C}_l . After $U_r \geq 9.5$, the \bar{y}/D of two downstream cylinders become much closer to each other in Regime V. Although the \bar{C}_l of downstream cylinders declines with increasing U_r , the lateral shifts of the \bar{y}/D increase. This can be attributed to the fact that in this study U_r is altered by reducing the spring stiffness.

Fig. 6 depicts the phase lags between the cylinder vibrations versus U_r . The phase lag ($\varphi_{2,3}$) between the oscillations of Cylinders 2 and 3 is in anti-phase in Regimes II and III but in in-phase in Regimes IV and V.

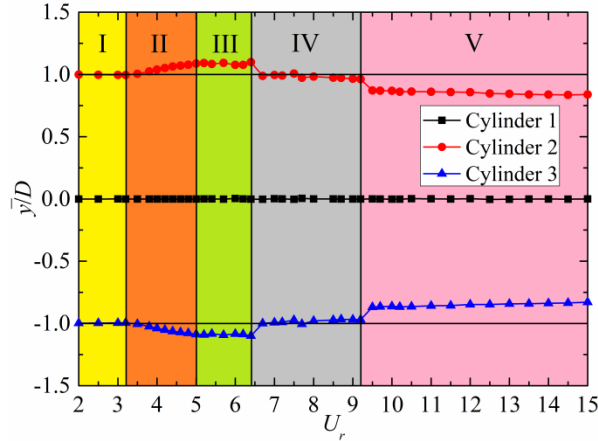
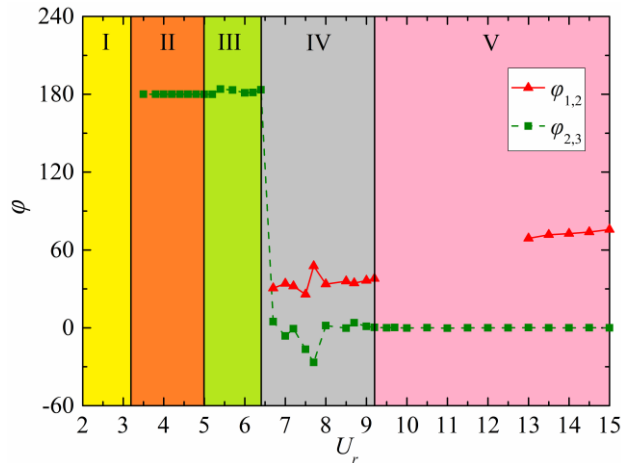


Fig. 5 The equilibrium positions of three cylinders

Fig. 6 The phase lag between the oscillations of three cylinders. $\phi_{1,2}$ and $\phi_{2,3}$ represent the phase lags between Cylinders 1 and 2 and between Cylinders 2 and 3, respectively

The $\phi_{2,3}$ does not exist in Regime I owing to no-vibration of the cylinders. The phase lag ($\phi_{1,2}$) between the oscillations of Cylinders 1 and 2 exists only in Regime IV and a part of Regime V with $U_r = 13 - 15$, showing a generally increasing trend with U_r . Due to the inequivalent vibration frequencies of Cylinders 1 and 2, $\phi_{1,2}$ ceases to exist in other regimes.

3.2 Hydrodynamic force and vibration features

3.2.1 Regime I

The hydrodynamic forces and vibration response are in the flip-flopping (FF) pattern. As shown in Figs. 7(a) and 7(b), the C_d and C_l of two downstream cylinders show a waxing-and-waning variation. This feature is related to the flip-flopping gap-flow which biases towards one of the downstream cylinders and changes its direction intermittently and randomly. Figs. 7(e) and 7(f) show the normalized vorticity contours in the near wake at $U_r = 3.0$. At the instant of Fig. 7(e), the gap-flow slightly deflects toward Cylinder 2. However, at the instant of Fig. 7(f), the gap-flow flips over. The switching of the gap-flow can be

reflected by the variation of the vibration response and the fluid forces. The cylinder toward which the gap flow is deflected has a larger C_d , smaller fluctuating C_l and smaller fluctuating y/D , and vice versa. The flip-over time scale is highly dependent on the Reynolds number from hundreds of vortex-shedding periods in turbulent flow (Kim and Durbin 1988) to several vortex-shedding periods in laminar flow (Kang 2003). In this case, the power spectral density (PSD) of the lift coefficient suggests that the flip-over time scale is about $f_{i1} / (f_{i2} - f_{i1}) \approx 7$ vortex-shedding periods, where f_{i1} ($= 0.10668$) and f_{i2} ($= 0.12099$) are the first and second dominant frequencies of C_l , respectively.

3.2.2 Regime II

At a larger U_r , in Regime II, the displacement histories of two downstream cylinders are in an anti-phase pattern, as shown in Figs. 8(a) and 8(d). No perceivable vibration is observed on the upstream cylinder. The upstream shear layers alternately reattach on the gap-side surface (Figs. 8(b) and 8(e)) and freestream-side surface (Figs. 8(c) and 8(f)) of the downstream cylinders, matching the rhythm of vortex-shedding and transverse oscillations. The vortices

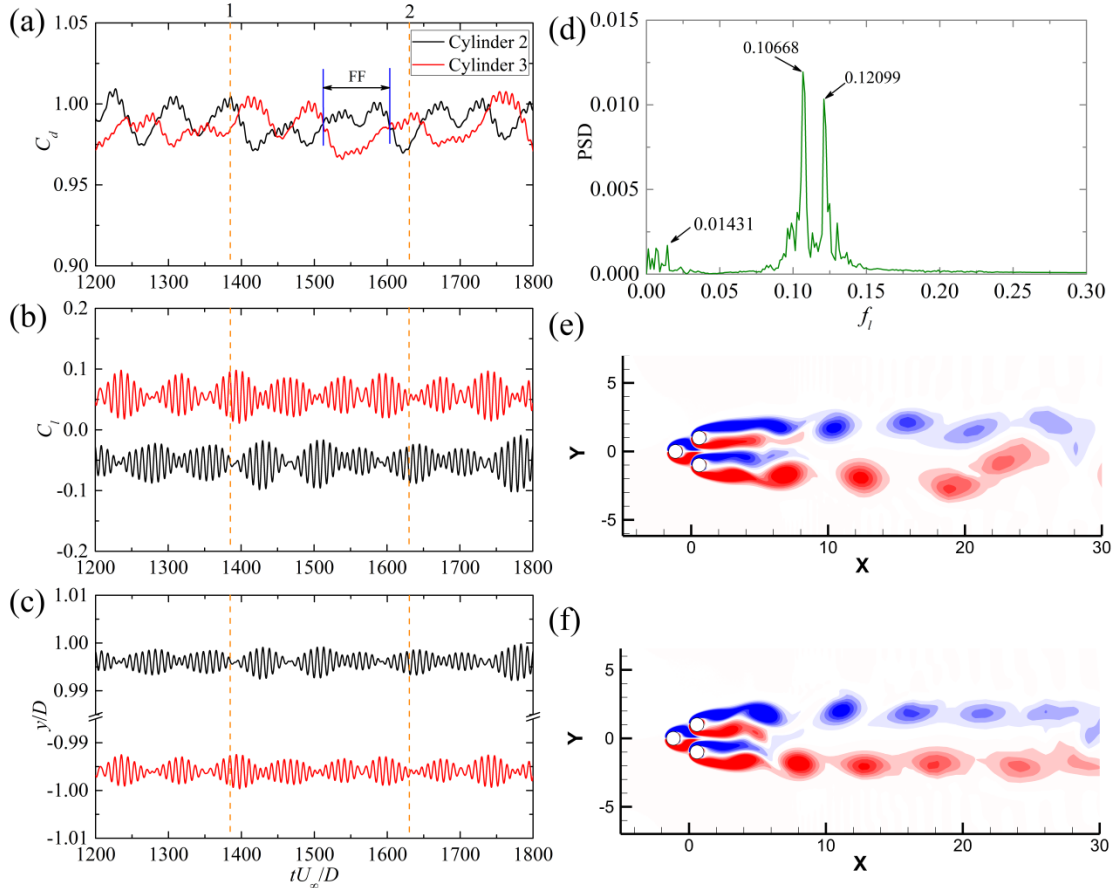


Fig. 7 Time histories of (a) drag coefficient, (b) lift coefficient and (c) displacement of two downstream cylinders at $U_r = 3.0$. (d) Power spectrum density (PSD) of the lift coefficients of downstream cylinders. (e)-(f) Vorticity contours at instants 1 and 2, marked in (a)-(c), when the gap flow deflects to Cylinder 2 and Cylinder 3, respectively. Arrows in (e), (f) indicate the gap flow directions

shed from the gap-side are rather weaker and smaller than those from the other side and quickly disappear in a short downstream distance. In the far wake, only two rows of parallel vortices are observed. With the increasing U_r , the symmetry of the wake is improved, from the staggered vortex-shedding at $U_r = 4.0$ to the aligned one at $U_r = 5.0$. Upon closer inspection, it can be found that the vortex-shedding at $U_r = 4.0$ is in the 2C pattern, i.e., one pair of co-rotating vortices shed from the freestream-side of a downstream cylinder in one oscillation period. The freestream side of the other downstream cylinder sheds another pair of co-rotating vortices. The co-rotating vortices merge in a short distance, which leads to the staggered vortex-shedding pattern in the far wake (Figs. 8(b) and 8(c)). As a result, the displacement spectrum of the upstream cylinder shows a dominant frequency at $f_y = 0.087$ which is half of the dominant frequency of the downstream cylinders at $f_y = 0.174$. However, at $U_r = 5.0$, the 2S pattern – two single vortices simultaneously shed from the freestream-side – occurs and a symmetric vortex-shedding is established.

3.2.3 Regime III

In this regime, the vibration of two downstream cylinders is out of tune and the wake is irregular. Fig. 9(a)

shows the time histories of the displacement of three cylinders at $U_r = 6.4$. It can be seen that the displacements of the downstream cylinders show a beating-like variation while the upstream cylinder displays a swaying envelope. Clearly, the short-time mean position of the upstream cylinder oscillates at a period much longer than the vortex-shedding period. The upward or downward deflection of the short-time mean position matches the beating of the downstream cylinders. As shown in Fig. 9(a), when the short-time mean position of Cylinder 1 downshifts (closer to Cylinder 3), Cylinder 3's vibration amplitude augments while Cylinder 2's diminishes, and vice versa. Although the vibration frequencies of the downstream cylinders, averaged over a long time-span, are identical (see Fig. 9(b)), the short-time vibration frequencies of the downstream cylinders are different. Fig. 9(c) displays the amplitude spectra of three cylinders within the timespan between the two vertical dashed lines in Fig. 9(a). Obviously, Cylinders 1 and 3 have the same dominant frequency at $f_y = 0.119$ which is smaller than the dominant frequency of Cylinder 2 at $f_y = 0.127$. A possible reason is that during this period the balanced position of Cylinder 1 is downward-shifted and thus Cylinder 1 and Cylinder 3 are more like in a tandem arrangement. The vibration of Cylinder 3 seems to be captured by the vortex-shedding from Cylinder 1, as shown

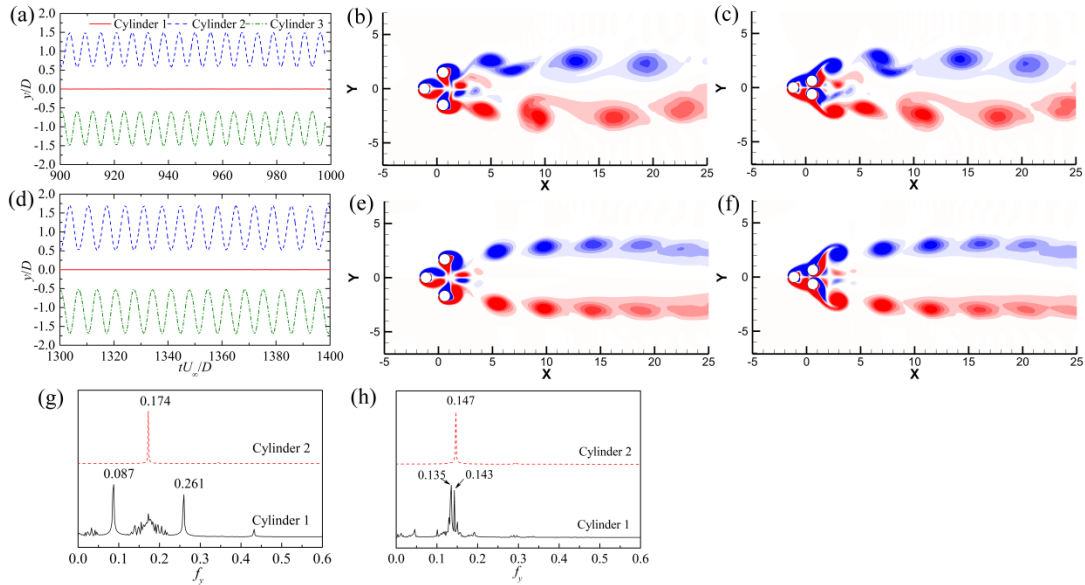


Fig. 8 (a), (d) Displacement histories, (b), (c), (e), (f) vorticity contours, and (g), (h) displacement spectra at $U_r = 4.0$ and 5.0 . Subplots (b), (c) and (e), (f) correspond to the instants of two downstream cylinders having maximum and minimum transverse separations, respectively

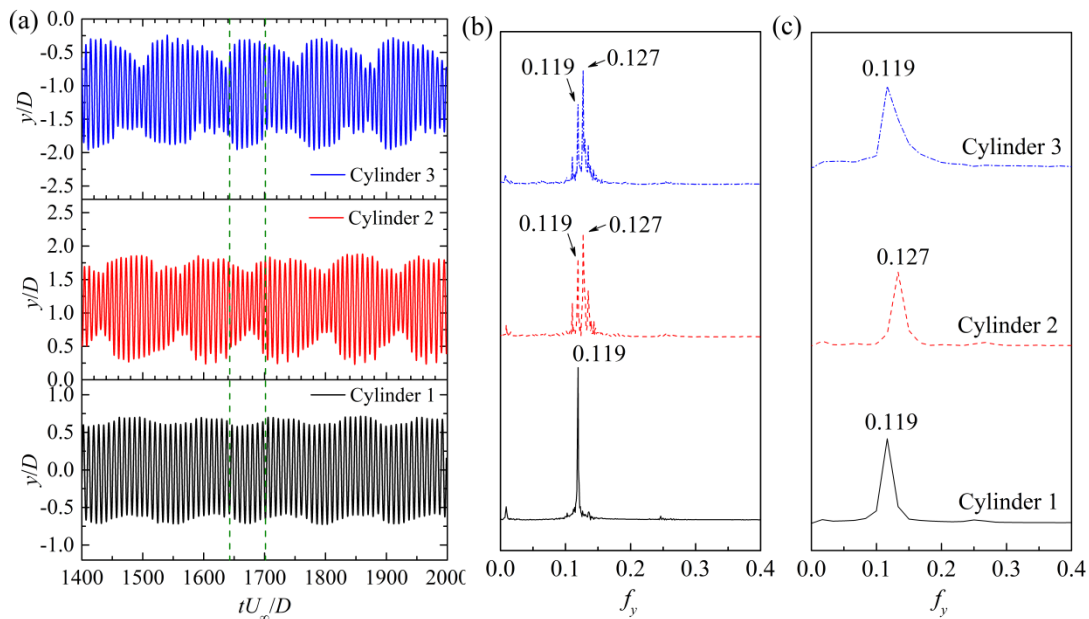


Fig. 9 Displacement histories (a), displacement spectra in the whole time-span (b) and between the vertical dashed lines (c) at $U_r = 6.4$

in Fig. 10. On the other hand, Cylinder 2 is less influenced by the wake of Cylinder 1 and has a different vibrating frequency.

3.2.4 Regime IV

In Regime IV, as shown in Fig. 11, the oscillations of two downstream cylinders are in in-phase and show a 30° phase difference with the oscillation of the upstream cylinder. Three cylinders have the same dominant vibration frequency and behave much like rigidly coupled bodies.

The vortex-shedding from the cylinders is a 2T pattern (see instants ii and iv in Fig. 11), that is, two triplets of vortices, with two co-rotating and one counter-rotating from a side, alternately generate in one vibration cycle. However, the counter-rotating vortex is much weaker and smaller than the co-rotating vortices from the same side and quickly vanishes. After the co-rotating vortices coalesce, the 2S vortex-shedding pattern establishes in the wake. The shear layers of the upstream cylinder merge with those of the downstream cylinders and boost the vortex-shedding from the downstream cylinders.

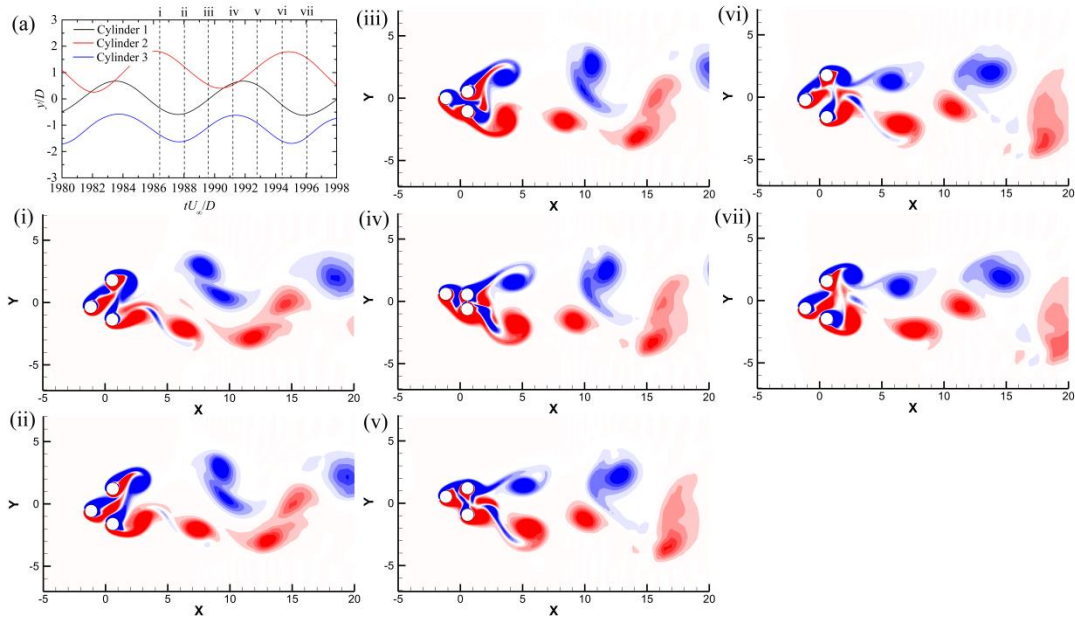


Fig. 10 Displacement histories (a) and vorticity contours (i-vii) at the instants marked in (a) at $U_r = 6.4$

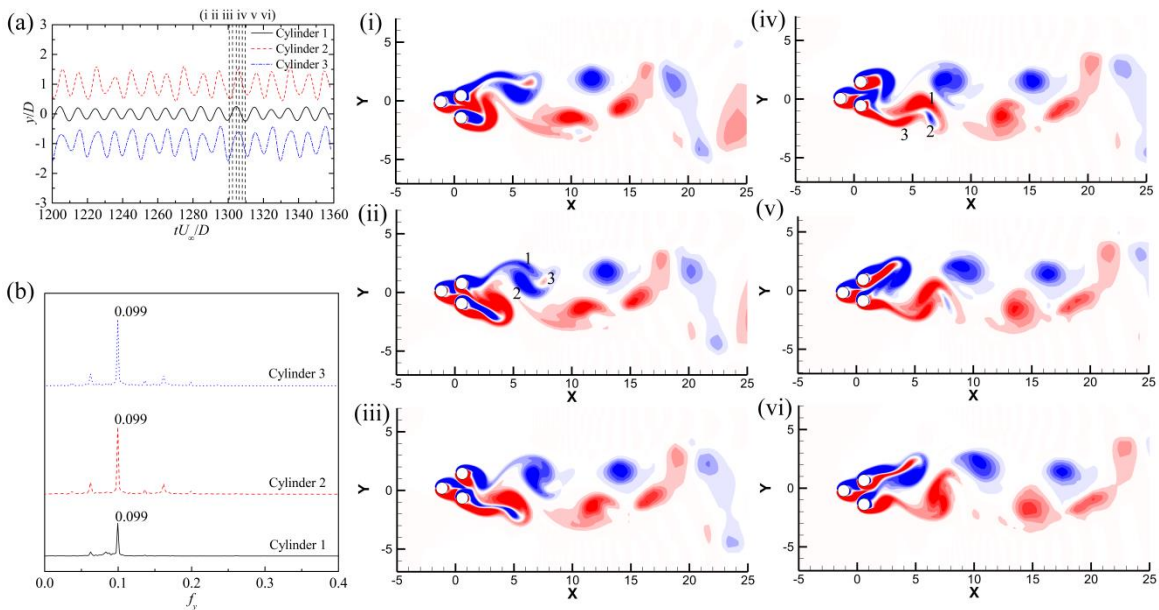


Fig. 11 Displacement histories, (b) displacement spectra of three cylinders at $U_r = 8.5$. Subplots (i-vi) show the vorticity contours at the instants marked in (a)

3.2.5 Regime V

The vibration pattern in Regime V is similar to that in Regime IV except that the beating-like vibration of the upstream cylinder is more significant, as shown in Fig. 12(a). This can also be reflected by the dual-peak displacement spectra of the upstream cylinder in Fig. 12(b). Different with the vortex-shedding pattern in Regime IV, the counter-rotating vortex ceases to exist which leads to a 2P pattern in Regime V. However, the 2P pattern is replaced by a 2S pattern after the co-rotating vortices merge.

4. Conclusions

Vortex-induced vibrations of three circular cylinders in an equilateral triangular arrangement were numerically studied. The center-to-center spacing ratio is $L/D = 2.0$, the Reynolds number is $Re = 100$, and the mass ratio is $m^* = 2.0$. Three cylinders are free to vibrate in the cross-flow direction. The numerical methodology was first validated in the case of VIV of three circular cylinders in an isosceles triangle arrangement. Good agreement with published data was achieved. Then the vibration response and hydrodynamic forces at different reduced velocities were

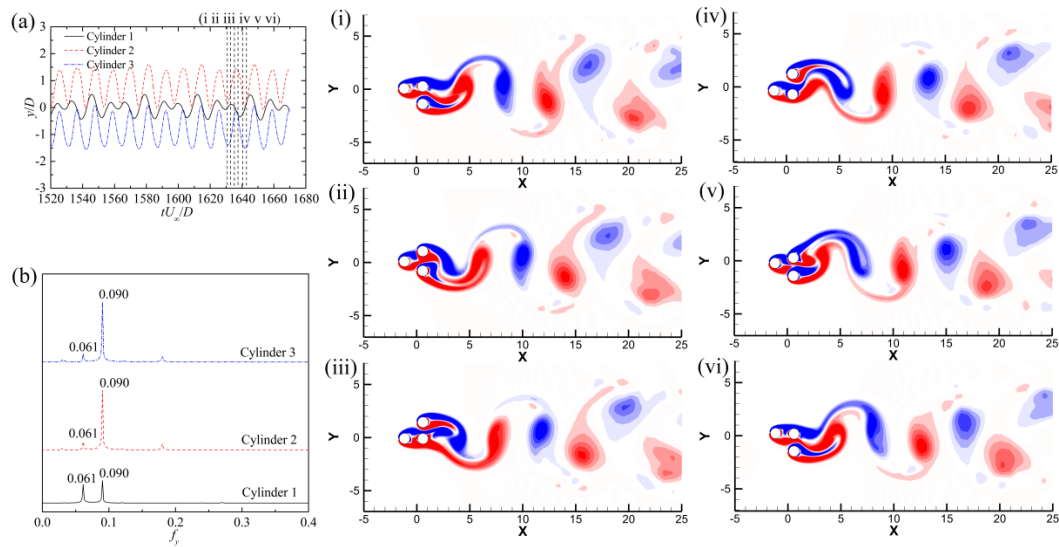


Fig. 12 (a) Displacement histories, (b) displacement spectra, and (i-iv) vorticity contours at the instants marked in (a). $U_r = 13.5$

investigated. The main conclusions are summarized as follows.

The vibration response is divided into five regimes according to the features of the vibration amplitude and the hydrodynamic forces.

In Regime I ($U_r \leq 3.2$), the vibration amplitudes of three cylinders are almost zero, and the corresponding wake undergoes a flip-flopping pattern. The gap flow between the two downstream cylinders changes its direction randomly and occasionally with a long switching period.

In Regime II ($3.2 < U_r \leq 5.0$), the amplitudes of the downstream cylinders increase significantly with U_r while the upstream cylinder amplitude keeps negligible. The vibrations of the downstream cylinders are in anti-phase which leads to a parallel vortex street. Large repulsive mean lift acts on the downstream cylinders.

In Regime III ($5.0 < U_r \leq 6.4$), the vibration amplitude of the upstream cylinder soars and approaches to those of the downstream cylinders. Local maximal amplitudes of three cylinders are obtained at the end of the range. The displacement histories of the downstream cylinders show a beating-like pattern while the short-time mean position of the upstream cylinder displays a long-period swinging. When the short-time mean position of the upstream cylinder moves downwards, the vibration of Cylinder 3 is enhanced but the vibration of Cylinder 2 weakens, and vice versa.

In Regime IV ($6.4 < U_r \leq 9.2$), the vibration amplitudes of three cylinders plummet. The oscillations of two downstream cylinders are in in-phase and attractive mean lift commences at the beginning of the range. The vortex-shedding is the 2T pattern with the triplet consisting of two co-rotating vortices and one counter-rotating vortex. An asymmetric vibration region is confirmed in the range of $7.2 < U_r < 7.8$.

In Regime V ($U_r > 9.2$), the vibration amplitudes of the downstream cylinders show a divergent trend. The vibration pattern and vortex-shedding are similar to those in Regime IV.

Acknowledgments

This work was financially supported by the Science Fund for Creative Research Groups of the National Natural Science Foundation of China (Grant No. 51621092), the National Natural Science Foundation of China (Grants No. 51579175 and 51779172), and the Special Program for Applied Research on Super Computation of the NSFC-Guangdong Joint Fund (the second phase) under Grant No. U1501501.

References

- Alam, M.M. (2014), "The aerodynamics of a cylinder submerged in the wake of another", *J. Fluid. Struct.*, **51**, 393-400. <https://doi.org/10.1016/j.jfluidstructs.2014.08.003>.
- Alam, M.M. (2016), "Lift forces induced by the phase lag between the vortex sheddings from two tandem bluff bodies", *J. Fluid. Struct.*, **65**, 217-237. <https://doi.org/10.1016/j.jfluidstructs.2016.05.008>.
- Alam, M.M. and Kim, S. (2009), "Free vibration of two identical circular cylinders in staggered arrangement", *Fluid Dyn. Res.*, **41**(3), 035507.
- Alam, M.M. and Meyer, J.P. (2013), "Global aerodynamic instability of twin cylinders in cross flow", *J. Fluid. Struct.*, **41**, 135-145. <https://doi.org/10.1016/j.jfluidstructs.2013.03.007>.
- Assi, G.R.S., Bearman, P.W. and Meneghini, J.R. (2010), "On the wake-induced vibration of tandem circular cylinders: the vortex interaction excitation mechanism", *J. Fluid Mech.*, **661**, 365-401. <https://doi.org/10.1017/S0022112010003095>.
- Assi, G.R.S., Bearman, P.W., Carmo, B.S., Meneghini, J.R., Sherwin, S.J. and Willden, R.H.J. (2013), "The role of wake stiffness on the wake-induced vibration of the downstream cylinder of a tandem pair", *J. Fluid Mech.*, **718**, 210-245. <https://doi.org/10.1017/jfm.2012.606>.
- Assi, G.R.S., Meneghini, J.R., Aranha, J.A.P., Bearman, P.W. and Casaprima, E. (2006), "Experimental investigation of flow-induced vibration interference between two circular cylinders", *J. Fluid. Struct.*, **22**(6-7), 819-827. <https://doi.org/10.1016/j.jfluidstructs.2006.04.013>.

- Behara, S., Ravikanth, B. and Chandra, V. (2017), "Vortex-induced vibrations of three staggered circular cylinders at low Reynolds numbers", *Phys. Fluids*, **29**(8), 083606. <https://doi.org/10.1063/1.4998417>.
- Bhatt, R. and Alam, M.M. (2018), "Vibration of a square cylinder submerged in a wake", *J. Fluid Mech.*, **853**, 301-332. <https://doi.org/10.1017/jfm.2018.573>.
- Blevins, R.D. (1990), "Flow-Induced Vibrations," Van Nostrand Reinhold, New York.
- Bokaian, A. and Geoola, F. (1984a), "Wake-induced galloping of two interfering circular cylinders", *J. Fluid Mech.*, **146**, 383-415. <https://doi.org/10.1017/S0022112084001920>
- Bokaian, A. and Geoola, F. (1984b), "Proximity-induced galloping of two interfering circular cylinders", *J. Fluid Mech.*, **146**, 417-449. <https://doi.org/10.1017/S0022112084001932>.
- Brika, D. and Laneville, A. (1999), "The flow interaction between a stationary cylinder and a downstream flexible cylinder", *J. Fluid. Struct.*, **13**(5), 579-606. <https://doi.org/10.1006/jfls.1999.0220>.
- Chen, W., Ji, C., Xu, W., Liu, S. and Campbell, J. (2015a), "Response and wake patterns of two side-by-side elastically supported circular cylinders in uniform laminar cross-flow", *J. Fluid. Struct.*, **55**, 218-236. <https://doi.org/10.1016/j.jfluidstructs.2015.03.002>.
- Chen, W., Ji, C., Wang, R., Xu, D. and Campbell, J. (2015b), "Flow-induced vibrations of two side-by-side circular cylinders: Asymmetric vibration, symmetry hysteresis and near-wake patterns", *Ocean Eng.*, **110**, 244-257. <https://doi.org/10.1016/j.oceaneng.2015.10.028>.
- Chen, W., Ji, C., Williams, J., Xu, D., Yang, L. and Cui, Y. (2018), "Vortex-induced vibrations of three tandem cylinders in laminar cross-flow: Vibration response and galloping mechanism", *J. Fluid. Struct.*, **78**, 215-238. <https://doi.org/10.1016/j.jfluidstructs.2017.12.017>.
- Flemming, F. and Williamson, C.H.K. (2005), "Vortex-induced vibrations of a pivoted cylinder", *J. Fluid Mech.*, **522**, 215-252. <https://doi.org/10.1017/S0022112004001831>.
- Hover, F.S. and Triantafyllou, M.S. (2001), "Galloping response of a cylinder with upstream wake interference", *J. Fluid. Struct.*, **15**(3-4), 503-512. <https://doi.org/10.1006/jfls.2000.0364>.
- Ji, C., Xiao, Z., Wang, Y. and Wang, H. (2011), "Numerical investigation on vortex-induced vibration of an elastically mounted circular cylinder at low Reynolds number using the fictitious domain method", *Int. J. Comput. Fluid D.*, **25**(4), 207-221. <https://doi.org/10.1080/10618562.2011.577034>.
- Ji, C., Munjiza, A. and Williams, J.J.R. (2012), "A novel iterative direct-forcing immersed boundary method and its finite volume applications", *J. Comput. Phys.*, **231**(4), 1797-1821. <https://doi.org/10.1016/j.jcp.2011.11.010>.
- Ji, C., Peng, Z., Alam M.M., Chen, W. and Xu, D. (2018a), "Vortex-induced vibration of a long flexible cylinder in uniform cross-flow", *Wind Struct.*, **26**(5), 267-277. <https://doi.org/10.12989/was.2018.26.5.267>.
- Ji, C., Xu, W., Sun, H., Wang, R., Ma, C. and Bernitsas, M.M. (2018b), "Interactive flow-induced vibrations of two staggered, low mass-ratio cylinders in the TrSL3 flow regime ($2.5 \times 10^4 < Re < 1.2 \times 10^5$): smooth cylinders", *J. Offshore Mech. Arct.*, **140**(4), 041801. doi: 10.1115/1.4038936.
- Kang S. (2003), "Characteristics of flow over two circular cylinders in a side-by-side arrangement at low Reynolds numbers", *Phys. Fluids*, **15**(9), 2486-2498. <https://doi.org/10.1063/1.1596412>.
- Kim, H.J. and Durbin, P.A. (1988), "Investigation of the flow between a pair of circular beams in the flopping regime", *J. Fluid Mech.*, **196**, 431-448. <https://doi.org/10.1017/S0022112088002769>.
- Kim, S., Alam M.M., Sakamoto, H. and Zhou, Y. (2009), "Flow-induced vibrations of two circular cylinders in tandem arrangement. Part1: Characteristics of vibration", *J. Wind Eng. Ind. Aerod.*, **97**(5-6), 304-311. <https://doi.org/10.1016/j.jweia.2009.07.004>.
- Kim, S., Alam, M.M. and Maiti, D.K. (2018), "Wake and suppression of flow-induced vibration of a circular cylinder", *Ocean Eng.*, **151**, 298-307. <https://doi.org/10.1016/j.oceaneng.2018.01.043>.
- Kim, S., Alam, M.M. and Russel, M. (2016), "Aerodynamics of a cylinder in the wake of a V-shaped object", *Wind Struct.*, **23**(2), 143-155. <http://dx.doi.org/10.12989/was.2016.23.2.143>.
- Kim, S. and Alam, M.M., (2015), "Characteristics and suppression of flow-induced vibrations of two side-by-side circular cylinders", *J. Fluid. Struct.*, **54**, 629-642. <https://doi.org/10.1016/j.jfluidstructs.2015.01.004>.
- King, R. and Johns, D.J. (1976), "Wake interaction experiments with two flexible circular cylinders in flowing water", *J. Sound Vib.*, **45**, 259-283. [https://doi.org/10.1016/0022-460X\(76\)90601-5](https://doi.org/10.1016/0022-460X(76)90601-5).
- Peskin, C.S. (1972), "Flow Patterns Around Heart Valves: a Digital Computer Method for Solving the Equations of Motion", Ph.D. Dissertation, Yeshiva University, New York.
- Qin, B., Alam, M.M. and Zhou, Y. (2017), "Two tandem cylinders of different diameters in crossflow: flow-induced vibration", *J. Fluid Mech.*, **829**, 621-658. <https://doi.org/10.1017/jfm.2017.510>
- Qin, B., Alam, M.M., Ji, C., Liu, Y. and Xu, S. (2018), "Flow-induced vibrations of two tandem cylinders of different natural frequencies", *Ocean Eng.*, **155**, 189-200.
- Sarpkaya, T. (2004), "A critical review of the intrinsic nature of vortex-induced vibrations", *J. Fluid. Struct.*, **19**(4), 389-447. <https://doi.org/10.1016/j.jfluidstructs.2004.02.005>.
- Williamson, C.H.K. and Govardhan, R. (2004), "Vortex-induced vibrations", *Annu. Rev. Fluid Mech.*, **36**, 413-455. <https://doi.org/10.1146/annurev.fluid.36.050802.122128>.
- Yu, K.R., Étienne, S., Scolan, Y-M., Hay, A., Fontaine, E. and Pelletier, D. (2016), "Flow-induced vibrations of in-line cylinder arrangements at low Reynolds numbers", *J. Fluid. Struct.*, **60**, 37-61. <https://doi.org/10.1016/j.jfluidstructs.2015.10.005>.
- Zdravkovich, M.M. (1977), "Review of flow interference between two circular cylinders in various arrangements", *J. Fluid Eng.*, **99**(4), 618-633. doi:10.1115/1.3448871.